Precision measurements of the $e^+e^- \to K_S^0 K^\pm \pi^\mp$ Born cross sections at center-of-mass energies between 3.8 and 4.6 GeV

M. Ablikim,[1] M. N. Achasov,[9,d] S. Ahmed,[14] M. Albrecht,[4] M. Alekseev,[55a,55c] A. Amoroso,[55a,55c] F. F. An,[1] Q. An,[52,42] Y. Bai,[41] O. Bakina,[26] R. Baldini Ferroli,[22a] Y. Ban,[34] D. W. Bennett,[21] J. V. Bennett,[5] N. Berger,[25] M. Bertani,[22a] D. Bettoni,[23a] F. Bianchi,[55a,55c] E. Boger,[26,b] I. Boyko,[26] R. A. Briere,[5] H. Cai,[57] X. Cai,[1,42] O. Cakir,[45a] A. Calcaterra,[22a] G. F. Cao,[1,46] S. A. Cetin,[45b] J. Chai,[55c] J. F. Chang,[1,42] G. Chelkov,[26,b,c] G. Chen,[1] H. S. Chen,[1,46] J. C. Chen,[1] M. L. Chen,[1,42] P. L. Chen,[53] S. J. Chen,[32] X. R. Chen,[29] Y. B. Chen,[1,42] X. K. Chu,[34] G. Cibinetto,[23a] F. Cossio,[55c] H. L. Dai,[1,42] J. P. Dai,[37,h] A. Dbeyssi,[14] D. Dedovich,[26] Z. Y. Deng,[1] A. Denig,[25] I. Denysenko,[26] M. Destefanis,[55a,55c] F. De Mori,[55a,55c] Y. Ding,[30] C. Dong,[33] J. Dong,[1,42] L. Y. Dong,[1,46] M. Y. Dong,[1,42,46] Z. L. Dou,[32] S. X. Du,[60] P. F. Duan,[1] J. Z. Fan,[44] J. Fang,[1,42] S. S. Fang,[1,46] Y. Fang,[1] R. Farinelli,[23a,23b] L. Fava,[55b,55c] S. Fegan,[25] F. Feldbauer,[4] G. Felici,[22a] C. Q. Feng,[52,42] E. Fioravanti,[23a] M. Fritsch,[4] C. D. Fu,[1] Q. Gao,[1] X. L. Gao,[52,42] Y. Gao,[44] Y. G. Gao,[6] Z. Gao,[52,42] B. Garillon,[25] I. Garzia,[23a] K. Goetzen,[10] L. Gong,[33] W. X. Gong,[1,42] W. Gradl,[25] M. Greco,[55a,55c] M. H. Gu,[1,42] S. Gu,[15] Y. T. Gu,[12] A. Q. Guo,[1] L. B. Guo,[31] R. P. Guo,[1,46] Y. P. Guo,[25] A. Guskov,[26] Z. Haddadi,[28] S. Han,[57] X. Q. Hao,[15] F. A. Harris,[47] K. L. He,[1,46] F. H. Heinsius,[4] T. Held,[4] Y. K. Heng,[1,42,46] T. Holtmann,[4] Z. L. Hou,[1] H. M. Hu,[1,46] J. F. Hu,[37,h] T. Hu,[1,42,46] Y. Hu,[1] G. S. Huang,[52,42] J. S. Huang,[15] X. T. Huang,[36] X. Z. Huang,[32] Z. L. Huang,[30] T. Hussain,[54] W. Ikegami Andersson,[56] Q. Ji,[1] Q. P. Ji,[15] X. B. Ji,[1,46] X. L. Ji,[1,42] X. S. Jiang,[1,42,46] X. Y. Jiang,[33] J. B. Jiao,[36] Z. Jiao,[17] D. P. Jin,[1,42,46] S. Jin,[1,46] Y. Jin,[48] T. Johansson,[56] A. Julin,[49] N. Kalantar-Nayestanaki,[28] X. S. Kang,[33] M. Kavatsyuk,[28] B. C. Ke,[5] T. Khan,[52,42] A. Khoukaz,[50] P. Kiese,[25] R. Kliemt,[10] L. Koch,[27] O. B. Kolcu,[45b,f] B. Kopf,[4] M. Kornicer,[47] M. Kuemmel,[4] M. Kuessner,[4] M. Kuhlmann,[4] A. Kupsc,[56] W. Kühn,[27] J. S. Lange,[27] M. Lara,[21] P. Larin,[14] L. Lavezzi,[55c] S. Leiber,[4] H. Leithoff,[25] C. Li,[56] Cheng Li,[52,42] D. M. Li,[60] F. Li,[1,42] F. Y. Li,[34] G. Li,[1] H. B. Li,[1,46] H. J. Li,[1,46] J. C. Li,[1] K. J. Li,[43] Kang Li,[13] Ke Li,[1] Lei Li,[3] P. L. Li,[52,42] P. R. Li,[46,7] Q. Y. Li,[36] T. Li,[36] W. D. Li,[1,46] W. G. Li,[1] X. L. Li,[36] X. N. Li,[1,42] X. Q. Li,[33] Z. B. Li,[43] H. Liang,[52,42] Y. F. Liang,[39] Y. T. Liang,[27] G. R. Liao,[11] J. Libby,[20] D. X. Lin,[14] B. Liu,[37,h] B. J. Liu,[1] C. X. Liu,[1] D. Liu,[52,42] F. H. Liu,[38] Fang Liu,[1] Feng Liu,[6] H. B. Liu,[12] H. M. Liu,[1,46] Huanhuan Liu,[1] Huihui Liu,[16] J. B. Liu,[52,42] J. Y. Liu,[1,46] K. Liu,[44] K. Y. Liu,[30] Ke Liu,[6] L. D. Liu,[34] Q. Liu,[46] S. B. Liu,[52,42] X. Liu,[29] Y. B. Liu,[33] Z. A. Liu,[1,42,46] Zhiqing Liu,[25] Y. F. Long,[34] X. C. Lou,[1,42,46] H. J. Lu,[17] J. G. Lu,[1,42] Y. Lu,[1] Y. P. Lu,[1,42] C. L. Luo,[31] M. X. Luo,[59] X. L. Luo,[1,42] S. Lusso,[55c] X. R. Lyu,[46] F. C. Ma,[30] H. L. Ma,[1] L. L. Ma,[36] M. M. Ma,[1,46] Q. M. Ma,[1] T. Ma,[1] X. N. Ma,[33] X. Y. Ma,[1,42] Y. M. Ma,[36] F. E. Maas,[14] M. Maggiora,[55a,55c] Q. A. Malik,[54] Y. J. Mao,[34] Z. P. Mao,[1] S. Marcello,[55a,55c] Z. X. Meng,[48] J. G. Messchendorp,[28] G. Mezzadri,[23a] J. Min,[1,42] T. J. Min,[1] R. E. Mitchell,[21] X. H. Mo,[1,42,46] Y. J. Mo,[6] C. Morales Morales,[14] G. Morello,[22a] N. Yu. Muchnoi,[9,d] H. Muramatsu,[49] A. Mustafa,[4] S. Nakhoul,[10,g] Y. Nefedov,[26] F. Nerling,[10,g] I. B. Nikolaev,[9,d] Z. Ning,[1,42] S. Nisar,[8] S. L. Niu,[1,42] X. Y. Niu,[1,46] S. L. Olsen,[35,j] Q. Ouyang,[1,42,46] S. Pacetti,[22b] Y. Pan,[52,42] M. Papenbrock,[56] P. Patteri,[22a] M. Pelizaeus,[4] J. Pellegrino,[55a,55c] H. P. Peng,[52,42] K. Peters,[10,g] J. Pettersson,[56] J. L. Ping,[31] R. G. Ping,[1,46] A. Pitka,[4] R. Poling,[49] V. Prasad,[52,42] H. R. Qi,[2] M. Qi,[32] T. Y. Qi,[2] S. Qian,[1,42] C. F. Qiao,[46] N. Qin,[57] X. S. Qin,[4] Z. H. Qin,[1,42] J. F. Qiu,[1] K. H. Rashid,[54,i] C. F. Redmer,[25] M. Richter,[4] M. Ripka,[25] M. Rolo,[55c] G. Rong,[1,46] Ch. Rosner,[14] X. D. Ruan,[12] A. Sarantsev,[26,e] M. Savrié,[23b] C. Schnier,[4] K. Schoenning,[56] W. Shan,[18] X. Y. Shan,[52,42] M. Shao,[52,42] C. P. Shen,[2] P. X. Shen,[33,*] X. Y. Shen,[1,46] H. Y. Sheng,[1] X. Shi,[1,42] J. J. Song,[36] W. M. Song,[36] X. Y. Song,[1] S. Sosio,[55a,55c] C. Sowa,[4] S. Spataro,[55a,55c] G. X. Sun,[1] J. F. Sun,[15] L. Sun,[57] S. S. Sun,[1,46] X. H. Sun,[1] Y. J. Sun,[52,42] Y. K. Sun,[52,42] Y. Z. Sun,[1] Z. J. Sun,[1,42] Z. T. Sun,[21] Y. T. Tan,[52,42] C. J. Tang,[39] G. Y. Tang,[1] X. Tang,[1] I. Tapan,[45c] M. Tiemens,[28] B. Tsednee,[24] I. Uman,[45d] G. S. Varner,[47] B. Wang,[1] B. L. Wang,[46] D. Wang,[34] D. Y. Wang,[34] Dan Wang,[46] K. Wang,[1,42] L. L. Wang,[1] L. S. Wang,[1] M. Wang,[36] Meng Wang,[1,46] P. Wang,[1] P. L. Wang,[1] W. P. Wang,[52,42] X. F. Wang,[1] Y. D. Wang,[14] Y. F. Wang,[1,42,46] Y. Q. Wang,[25] Z. Wang,[1,42] Z. G. Wang,[1,42] Z. Y. Wang,[1] Zongyuan Wang,[1,46] T. Weber,[4] D. H. Wei,[11] P. Weidenkaff,[25] S. P. Wen,[1] U. Wiedner,[4] M. Wolke,[56] L. H. Wu,[1] L. J. Wu,[1,46] Z. Wu,[1,42] L. Xia,[52,42] X. Xia,[36] Y. Xia,[19] D. Xiao,[1] Y. J. Xiao,[1,46] Z. J. Xiao,[31] Y. G. Xie,[1,42] Y. H. Xie,[6] X. A. Xiong,[1,46] Q. L. Xiu,[1,42] G. F. Xu,[1] J. J. Xu,[1,46] L. Xu,[1] Q. J. Xu,[13] Q. N. Xu,[46] X. P. Xu,[40] L. Yan,[55a,55c] W. B. Yan,[52,42] W. C. Yan,[2] Y. H. Yan,[19] H. J. Yang,[37,h] H. X. Yang,[1] L. Yang,[57] Y. H. Yang,[32] Y. X. Yang,[11] Yifan Yang,[1,46] M. Ye,[1,42] M. H. Ye,[7] J. H. Yin,[1] Z. Y. You,[43] B. X. Yu,[1,42,46] C. X. Yu,[33] C. Z. Yuan,[1,46] Y. Yuan,[1] A. Yuncu,[45b,a] A. A. Zafar,[54] A. Zallo,[22a] Y. Zeng,[19] Z. Zeng,[52,42] B. X. Zhang,[1] B. Y. Zhang,[1,42] C. C. Zhang,[1] D. H. Zhang,[1] H. H. Zhang,[43] H. Y. Zhang,[1,42] J. Zhang,[1,46] J. L. Zhang,[58] J. Q. Zhang,[4] J. W. Zhang,[1,42,46] J. Y. Zhang,[1] J. Z. Zhang,[1,46] K. Zhang,[1,46] L. Zhang,[44] X. Y. Zhang,[36] Y. Zhang,[52,42] Y. H. Zhang,[1,42] Y. T. Zhang,[52,42] Yang Zhang,[1] Yao Zhang,[1] Yu Zhang,[46] Z. H. Zhang,[6] Z. P. Zhang,[52] Z. Y. Zhang,[57] G. Zhao,[1] J. W. Zhao,[1,42] J. Y. Zhao,[1,46] J. Z. Zhao,[1,42] Lei Zhao,[52,42] Ling Zhao,[1] M. G. Zhao,[33] Q. Zhao,[1] S. J. Zhao,[60] T. C. Zhao,[1] Y. B. Zhao,[1,42] Z. G. Zhao,[52,42] A. Zhemchugov,[26,b] B. Zheng,[53] J. P. Zheng,[1,42] W. J. Zheng,[36] Y. H. Zheng,[46] B. Zhong,[31] L. Zhou,[1,42] X. Zhou,[57] X. K. Zhou,[52,42] X. R. Zhou,[52,42] X. Y. Zhou,[1] Y. X. Zhou,[12] J. Zhu,[33]

J. Zhu,[43] K. Zhu,[1] K. J. Zhu,[1,42,46] S. Zhu,[1] S. H. Zhu,[51] X. L. Zhu,[44] Y. C. Zhu,[52,42] Y. S. Zhu,[1,46] Z. A. Zhu,[1,46] J. Zhuang,[1,42] B. S. Zou,[1] and J. H. Zou[1]

(BESIII Collaboration)

[1]*Institute of High Energy Physics, Beijing 100049, People's Republic of China*
[2]*Beihang University, Beijing 100191, People's Republic of China*
[3]*Beijing Institute of Petrochemical Technology, Beijing 102617, People's Republic of China*
[4]*Bochum Ruhr-University, D-44780 Bochum, Germany*
[5]*Carnegie Mellon University, Pittsburgh, Pennsylvania 15213, USA*
[6]*Central China Normal University, Wuhan 430079, People's Republic of China*
[7]*China Center of Advanced Science and Technology, Beijing 100190, People's Republic of China*
[8]*COMSATS Institute of Information Technology, Lahore, Defence Road, Off Raiwind Road, 54000 Lahore, Pakistan*
[9]*G.I. Budker Institute of Nuclear Physics SB RAS (BINP), Novosibirsk 630090, Russia*
[10]*GSI Helmholtzcentre for Heavy Ion Research GmbH, D-64291 Darmstadt, Germany*
[11]*Guangxi Normal University, Guilin 541004, People's Republic of China*
[12]*Guangxi University, Nanning 530004, People's Republic of China*
[13]*Hangzhou Normal University, Hangzhou 310036, People's Republic of China*
[14]*Helmholtz Institute Mainz, Johann-Joachim-Becher-Weg 45, D-55099 Mainz, Germany*
[15]*Henan Normal University, Xinxiang 453007, People's Republic of China*
[16]*Henan University of Science and Technology, Luoyang 471003, People's Republic of China*
[17]*Huangshan College, Huangshan 245000, People's Republic of China*
[18]*Hunan Normal University, Changsha 410081, People's Republic of China*
[19]*Hunan University, Changsha 410082, People's Republic of China*
[20]*Indian Institute of Technology Madras, Chennai 600036, India*
[21]*Indiana University, Bloomington, Indiana 47405, USA*
[22a]*INFN Laboratori Nazionali di Frascati, I-00044, Frascati, Italy*
[22b]*INFN and University of Perugia, I-06100, Perugia, Italy*
[23a]*INFN Sezione di Ferrara, I-44122, Ferrara, Italy*
[23b]*University of Ferrara, I-44122, Ferrara, Italy*
[24]*Institute of Physics and Technology, Peace Ave. 54B, Ulaanbaatar 13330, Mongolia*
[25]*Johannes Gutenberg University of Mainz, Johann-Joachim-Becher-Weg 45, D-55099 Mainz, Germany*
[26]*Joint Institute for Nuclear Research, 141980 Dubna, Moscow region, Russia*
[27]*Justus-Liebig-Universitaet Giessen, II. Physikalisches Institut, Heinrich-Buff-Ring 16, D-35392 Giessen, Germany*
[28]*KVI-CART, University of Groningen, NL-9747 AA Groningen, The Netherlands*
[29]*Lanzhou University, Lanzhou 730000, People's Republic of China*
[30]*Liaoning University, Shenyang 110036, People's Republic of China*
[31]*Nanjing Normal University, Nanjing 210023, People's Republic of China*
[32]*Nanjing University, Nanjing 210093, People's Republic of China*
[33]*Nankai University, Tianjin 300071, People's Republic of China*
[34]*Peking University, Beijing 100871, People's Republic of China*
[35]*Seoul National University, Seoul, 151-747, Korea*
[36]*Shandong University, Jinan 250100, People's Republic of China*
[37]*Shanghai Jiao Tong University, Shanghai 200240, People's Republic of China*
[38]*Shanxi University, Taiyuan 030006, People's Republic of China*
[39]*Sichuan University, Chengdu 610064, People's Republic of China*
[40]*Soochow University, Suzhou 215006, People's Republic of China*
[41]*Southeast University, Nanjing 211100, People's Republic of China*
[42]*State Key Laboratory of Particle Detection and Electronics, Beijing 100049, Hefei 230026, People's Republic of China*
[43]*Sun Yat-Sen University, Guangzhou 510275, People's Republic of China*
[44]*Tsinghua University, Beijing 100084, People's Republic of China*
[45a]*Ankara University, 06100 Tandogan, Ankara, Turkey*
[45b]*Istanbul Bilgi University, 34060 Eyup, Istanbul, Turkey*
[45c]*Uludag University, 16059 Bursa, Turkey*
[45d]*Near East University, Nicosia, North Cyprus, Mersin 10, Turkey*
[46]*University of Chinese Academy of Sciences, Beijing 100049, People's Republic of China*
[47]*University of Hawaii, Honolulu, Hawaii 96822, USA*

[48]University of Jinan, Jinan 250022, People's Republic of China
[49]University of Minnesota, Minneapolis, Minnesota 55455, USA
[50]University of Muenster, Wilhelm-Klemm-Str. 9, 48149 Muenster, Germany
[51]University of Science and Technology Liaoning, Anshan 114051, People's Republic of China
[52]University of Science and Technology of China, Hefei 230026, People's Republic of China
[53]University of South China, Hengyang 421001, People's Republic of China
[54]University of the Punjab, Lahore - 54590, Pakistan
[55a]University of Turin, I-10125, Turin, Italy
[55b]University of Eastern Piedmont, I-15121, Alessandria, Italy
[55c]INFN, I-10125, Turin, Italy
[56]Uppsala University, Box 516, SE-75120 Uppsala, Sweden
[57]Wuhan University, Wuhan 430072, People's Republic of China
[58]Xinyang Normal University, Xinyang 464000, People's Republic of China
[59]Zhejiang University, Hangzhou 310027, People's Republic of China
[60]Zhengzhou University, Zhengzhou 450001, People's Republic of China

(Received 29 August 2018; published 11 April 2019)

Using data samples collected by the BESIII detector operating at the BEPCII storage ring, we measure the $e^+e^- \to K_S^0 K^\pm \pi^\mp$ Born cross sections at center-of-mass energies between 3.8 and 4.6 GeV, corresponding to a luminosity of about 5.0 fb^{-1}. The results are compatible with the *BABAR* measurements, but with the precision significantly improved. A simple $1/s^n$ dependence for the continuum process can describe the measured cross sections, but a better fit is obtained by an additional resonance near 4.2 GeV, which could be an excited charmonium or a charmoniumlike state.

DOI: 10.1103/PhysRevD.99.072005

I. INTRODUCTION

The charmoniumlike state $Y(4260)$ was first observed in the initial state radiation (ISR) process, $e^+e^- \to \gamma_{\mathrm{ISR}}\pi^+\pi^- J/\psi$, by *BABAR* [1], and later confirmed by the CLEO [2] and Belle [3] experiments. In 2016, a resonant structure, the $Y(4220)$, was observed in the process $e^+e^- \to \pi^+\pi^- h_c$ by the BESIII collaboration [4]. At the same time, BESIII reported a precise measurement of the $e^+e^- \to \pi^+\pi^- J/\psi$ cross sections in the center-of-mass (c.m.) energy region from 3.77 to 4.60 GeV [5], where it found the $Y(4260)$ to have a mass of $(4222.0 \pm 3.1 \pm 1.4)$ MeV/c^2 and a width of $(44.1 \pm 4.3 \pm 2.0)$ MeV, in good agreement with the $Y(4220)$ observed in $e^+e^- \to \pi^+\pi^- h_c$ [4]. Given the similar masses and widths, they may be the same particle, denoted thereafter as $Y(4220/4260)$. Since $Y(4220/4260)$ is produced in e^+e^- annihilation, its quantum numbers must be $J^{PC} = 1^{--}$. However, $Y(4220/4260)$ seems to have rather different properties compared with the known charmonium states with $J^{PC} = 1^{--}$ in the same mass region, such as $\psi(4040)$, $\psi(4160)$, and $\psi(4415)$ [6–8]. Although above $D\bar{D}$ production threshold, the $Y(4220/4260)$ has strong coupling to the $\pi^+\pi^- J/\psi$ final state, instead of the $D^{(*)}\bar{D}^{(*)}$ final state [9]. Such a strong coupling to a hidden-charm final state suggests that the $Y(4220/4260)$ is a nonconventional $c\bar{c}$ meson. Various scenarios have been proposed, which interpret the $Y(4220/4260)$ as a tetraquark state, hybrid state, molecular state, or dynamical effect [10–14], but all need to be tested with experimental data. Most previous studies of the $Y(4220/4260)$ are based on hadronic transitions. The CLEO experiment investigated 16 charmonium and light hadron decay modes based on 13.2 pb^{-1} of e^+e^- data collected at c.m. energy of $\sqrt{s} = 4.260$ GeV,

[*]Corresponding author.
shenpx@mail.nankai.edu.cn
[a]Also at Bogazici University, 34342 Istanbul, Turkey.
[b]Also at the Moscow Institute of Physics and Technology, Moscow 141700, Russia.
[c]Also at the Functional Electronics Laboratory, Tomsk State University, Tomsk, 634050, Russia.
[d]Also at the Novosibirsk State University, Novosibirsk, 630090, Russia.
[e]Also at the NRC "Kurchatov Institute", PNPI, 188300, Gatchina, Russia.
[f]Also at Istanbul Arel University, 34295 Istanbul, Turkey.
[g]Also at Goethe University Frankfurt, 60323 Frankfurt am Main, Germany.
[h]Also at Key Laboratory for Particle Physics, Astrophysics and Cosmology, Ministry of Education; Shanghai Key Laboratory for Particle Physics and Cosmology; Institute of Nuclear and Particle Physics, Shanghai 200240, People's Republic of China.
[i]Also at Government College Women University, Sialkot - 51310, Punjab, Pakistan.
[j]Present address: Center for Underground Physics, Institute for Basic Science, Daejeon 34126, Korea.

TABLE I. The measured $e^+e^- \to K_S^0 K^+ \pi^-$ Born cross sections. Shown in the table are the integrated luminosities $\mathcal{L}$, the numbers of events in the signal region N^{obs}, the numbers of estimated background events N^{bkg}, the signal yields $N^{\text{sig}} = N^{\text{obs}} - N^{\text{bkg}}$, the detection efficiencies ϵ, the ISR correction factors $(1+\delta^{\text{ISR}})$, the vacuum polarization correction factors $\frac{1}{|1-\Pi|^2}$ and the measured Born cross sections σ_B. The first uncertainty on the cross section is statistical and the second systematic.

$\sqrt{s}$ (GeV)	$\mathcal{L}$ (pb^{-1})	N^{obs}	N^{bkg}	N^{sig}	ε (%)	$(1+\delta^{\text{ISR}})$	$\frac{1}{\|1-\Pi\|^2}$	σ_B (pb)
3.808	50.1	151	0.0	151.0	26.4	0.901	1.054	$17.38 \pm 1.41 \pm 0.77$
3.896	52.6	92	1.0	91.0	28.1	0.847	1.047	$10.05 \pm 1.07 \pm 0.44$
4.008	480.5	795	11.8	783.2	28.8	0.844	1.043	$9.29 \pm 0.34 \pm 0.41$
4.086	52.4	78	3.0	75.0	27.1	0.843	1.052	$8.62 \pm 1.04 \pm 0.38$
4.189	43.1	70	1.0	69.0	27.8	0.840	1.056	$9.39 \pm 1.15 \pm 0.41$
4.208	54.3	71	1.0	70.0	27.1	0.840	1.057	$7.75 \pm 0.94 \pm 0.34$
4.217	54.2	80	2.0	78.0	27.8	0.840	1.057	$8.43 \pm 0.98 \pm 0.37$
4.226	1041.6	1343	25.3	1317.7	26.9	0.840	1.056	$7.67 \pm 0.22 \pm 0.34$
4.242	55.5	70	4.0	66.0	26.4	0.839	1.056	$7.35 \pm 0.96 \pm 0.32$
4.258	825.7	960	18.8	941.2	26.9	0.839	1.052	$6.94 \pm 0.23 \pm 0.31$
4.308	45.3	40	1.0	39.0	26.5	0.838	1.054	$5.32 \pm 0.87 \pm 0.23$
4.358	541.4	538	19.5	518.5	26.4	0.837	1.051	$5.97 \pm 0.27 \pm 0.26$
4.387	55.3	54	4.0	50.0	26.7	0.836	1.051	$5.58 \pm 0.85 \pm 0.25$
4.416	1029.6	949	20.8	928.2	27.0	0.836	1.053	$5.49 \pm 0.18 \pm 0.24$
4.600	566.9	395	16.4	378.6	25.8	0.832	1.054	$4.27 \pm 0.23 \pm 0.19$

but only a few decay modes had significance greater than 3σ [15]. The *BABAR* collaboration has measured the cross section of $e^+e^- \to K_S^0 K^\pm \pi^\mp$ [16] with the ISR process and found an excess around $\sqrt{s} = 4.2$ GeV, which is very close to the $\psi(4160)$ and $Y(4220/4260)$. Analyzing this process with a larger data sample provides higher precision and more information on $Y(4220/4260)$ decays to light hadrons.

In this paper, we report measurements of the $e^+e^- \to K_S^0 K^+ \pi^-$, $K_S^0 \to \pi^+\pi^-$ Born cross section at c.m. energies from 3.8 to 4.6 GeV. The charge conjugate decays to $K_S^0 K^- \pi^+$ are included in this analysis. The corresponding c.m. energies [17] and the integrated luminosities [18] of all the data samples used in this paper are summarized in Table I.

II. DETECTOR AND MONTE-CARLO SIMULATION

The BESIII detector [19] at the BEPCII collider [20] is a large solid-angle magnetic spectrometer with a geometrical acceptance of 93% of 4π. It has four main components: (1) A small-cell, helium-based (60% He, 40% C_3H_8) multilayer drift chamber (MDC) with 43 layers providing an average single-hit resolution of 135 μm, a charged-particle momentum resolution in a 1.0 T magnetic field of 0.5% at 1.0 GeV$/c$ and a dE/dx resolution better than 6%; (2) A time-of-flight system (TOF) constructed of 5 cm thick plastic scintillator, with 176 detectors of 2.4 m length in two layers in the barrel and 96 fan-shaped detectors in the endcaps. The barrel (endcap) time resolution of 80 ps (110 ps) provides a 2σ K/π separation for momenta up to $\sim$1.0 GeV$/c$; (3) An electromagnetic calorimeter (EMC) consisting of 6240 CsI(Tl) crystals in a cylindrical structure (barrel) and two endcaps. The energy and the position resolutions for 1.0 GeV photon are 2.5% (5%) and 6 mm (9 mm) in the barrel (endcaps), respectively; (4) A muon system (MUC) consisting of resistive plate chambers in nine barrel and eight endcap layers, which provides a 2 cm position resolution.

To study the backgrounds and determine the detection efficiencies, a GEANT4-based [21] Monte-Carlo (MC) simulation package is used, which includes the geometric and material description of the BESIII detector, the detector response, and the digitization models, as well as the detector running conditions and performance. Signal MC samples of $e^+e^- \to K_S^0 K^+ \pi^-$ are generated with phase space (PHSP) distributions with EVTGEN [22,23], which includes ISR effects [24]. The PHSP signal MC samples are reweighted according to the results from the partial wave analysis (PWA) presented later in the paper. For the ISR calculation, the $e^+e^- \to K_S^0 K^+ \pi^-$ Born cross section results from *BABAR* [16] are taken as the initial input, and the energy of the ISR photon is required to be less than 0.1 GeV since the events with large energy ISR photons cannot survive the event selection. For the background study, an inclusive MC sample with integrated luminosity equivalent to data is generated, including open charm, low-mass vector charmonium states produced by ISR, continuum light quark states, and other quantum electrodynamics (QED) processes. The known decay modes of the charmonium states are produced with EVTGEN [22,23] according to the world average branching fraction (BF) values from the Particle Data Group (PDG) [25], while the unknown decay modes are generated with the LUNDCHARM generator [26].

III. DATA ANALYSIS

The signal candidates of the $e^+e^- \to K_S^0 K^+ \pi^-$ process are selected by requiring a K_S^0 candidate and a kaon and pion pair with a net charge of zero.

The charged kaon and pion candidates, reconstructed using hits in the MDC, are required to be within the polar angle range $|\cos\theta| < 0.93$ and pass within a cylindrical region extending ± 10 cm from the average interaction point (IP) of each run along the beam direction and with a 1 cm radius perpendicular to the beam direction. The time information from the TOF and the ionization measured in the MDC (dE/dx) are combined to calculate particle identification (PID) confidence levels (C.L.) for the K and π hypotheses, and the particle type with the highest C.L. is assigned to each track. An identified kaon and an identified pion with opposite electric charge are required.

The K_S^0 candidate is reconstructed with a pair of oppositely charged tracks, which are assumed to be pions. Their distances of closest approach to the IP must be within 25 cm and 20 cm along the beam direction and in the transverse plane, respectively. Then primary and secondary vertex fits [27] are performed, and the decay length of the secondary vertex is required to be greater than twice its uncertainty. The invariant mass of $\pi^+\pi^-$, $m_{\pi^+\pi^-}$, must satisfy $|m_{\pi^+\pi^-} - M_{K_S^0}| < 0.020$ GeV$/c^2$, where $M_{K_S^0}$ is the world average of the K_S^0 mass [25]. To suppress the background from photon conversion, the pions from the K_S^0 decay must satisfy $E/Pc < 0.8$, where E and P are the energy deposited in the EMC and the momentum measured in the MDC, respectively. If there are multiple K_S^0 candidates in an event, the one with the smallest χ^2 of the secondary vertex fit is taken.

To improve the momentum resolution and suppress background, a four constraint (4C) kinematic fit is performed by imposing energy-momentum conservation under the $e^+e^- \to K_S^0 K^+ \pi^-$ hypothesis, and its chi-square is required to be less than 40.

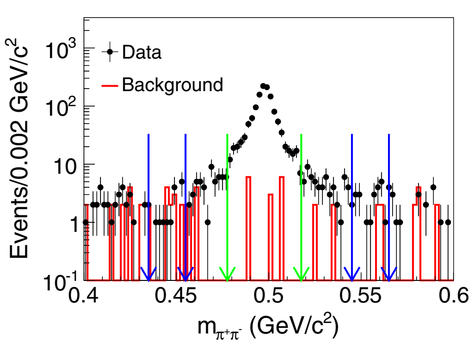

FIG. 1. The distribution of the $\pi^+\pi^-$ invariant mass for the data at $\sqrt{s} = 4.226$ GeV. The black dots with error bars are data, and the red histogram is background estimated from MC simulation. The blue arrows denote the sideband regions and green arrows shows the signal regions.

After all the event selection criteria are applied, the inclusive MC sample shows that the surviving background is found to be mainly from processes with (1) four charged tracks in the final state, e.g., $e^+e^- \to K^+K^-\pi^+\pi^-$, due to particle misidentification between the kaon and pion and (2) a radiative photon, e.g., $e^+e^- \to \gamma e^+e^-$, which converts into an electron-positron pair and the electron and positron are misidentified as a pion and a kaon. The signal yields, N^{sig}, are obtained by counting the events in the signal region $|m_{\pi^+\pi^-} - M_{K_S^0}| < 0.020$ GeV and the number of remaining background events, N^{bkg}, is evaluated using the events in the sideband regions, which are defined as $m_{\pi^+\pi^-} \in (0.435, 0.455) \cup (0.545, 0.565)$ GeV$/c^2$, as shown in Fig. 1. In the sideband region, there is still a small contribution from signal events, which is estimated with signal MC simulation and subtracted in the estimation of backgrounds.

Figure 2 (top) shows the Dalitz plot of the selected events at c.m. energy $\sqrt{s} = 4.226$ GeV. Two vertical bands, corresponding to the neutral $K^*(892)$ and $K_2^*(1430)$ decaying into $K^\pm\pi^\mp$, and a horizontal band, corresponding to the charged $K_2^*(1430)$ decaying into $K_S^0\pi^\pm$, are observed. There are also diagonal bands corresponding to the intermediate states, e.g., $a_2(1320)^\pm$ and excited $\rho^\pm$ with high mass, decaying into $K_S^0 K^\pm$. In order to obtain the detection efficiencies, PWAs are performed on the $K_S^0 K\pi$

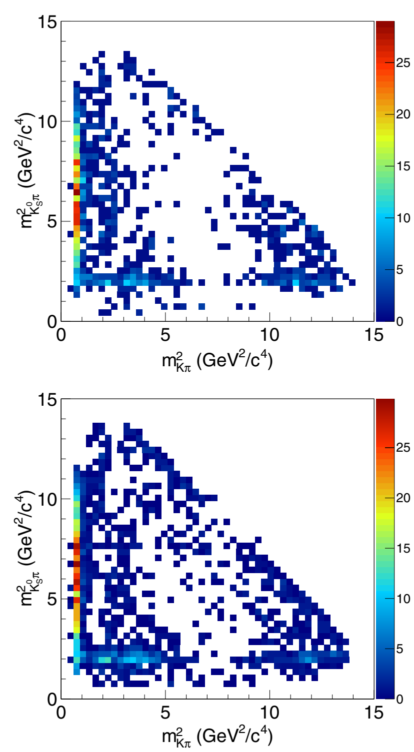

FIG. 2. The Dalitz plots of $e^+e^- \to K_S^0 K^+ \pi^-$ for the data at $\sqrt{s} = 4.226$ GeV. The top plot is data and the bottom one is MC simulation generated with the amplitude analysis results.

system at different c.m. energy points. The contributions of PHSP and possible intermediate states in the $K_S^0\pi$, $K\pi$, and K_S^0K systems, including $K^*(892)$, $K_2^*(1430)$, $K_3^*(1780)$, $a_2(1320)$, $\rho(1700)$, and $\rho(2150)$, are taken into account. In the PWAs, these intermediate states are described with relativistic Breit-Wigner (BW) functions with their masses and widths fixed to the world averages [25]. The amplitudes for the subsequent two body decays are constructed with the covariant helicity method [28,29]. For a particle decaying into a two-body final state, i.e., $A(J,m) \to B(s,\lambda)C(\sigma,\nu)$, its helicity amplitude $F^J_{\lambda,\nu}$ [28,29] is

$$F^J_{\lambda,\nu} = \sum_{LS} \sqrt{\frac{2L+1}{2J+1}} g_{LS} \langle L\alpha S\delta | J\delta \rangle \langle s\lambda\sigma - \nu | S\delta \rangle r^L \frac{B_L(r)}{B_L(r_0)}, \tag{1}$$

where J, s, and σ are the spins of A, B, and C, respectively; m, λ, and ν are their helicities, respectively; L and S are the total orbital angular momentum and spin of AB system, respectively; $\alpha = 0$; $\delta = \lambda - \nu$; g_{LS} is the coupling constant in the $L-S$ coupling scheme; the angular brackets denote Clebsch-Gordan coefficients; r is the magnitude of the momentum difference between the two final state particles in their mother's rest frame (r_0 corresponds to the momentum difference at the nominal mass of the resonance); and B_L is the barrier factor [30]. The magnitudes and relative phases of complex coupling constants g_{LS} are determined by an unbinned maximum likelihood fit to data with MINUIT [31], and the effect of backgrounds is subtracted from the likelihood as described in Ref. [32]. Figure 3 shows the fit results for the invariant mass distributions of $K\pi$, $K_S^0\pi$, and K_S^0K, as well as the polar angle distributions of π, K, and K_S^0 at $\sqrt{s} = 4.226$ GeV, where good agreement with data is seen. The situation of other data sets are similar. Then the detection efficiency ϵ is obtained by reweighting the signal PHSP MC sample of $e^+e^- \to K_S^0K^+\pi^-$ with the fitted PWA amplitude,

$$\epsilon = \frac{\sum_{i=1}^{N_{\rm MC}^{\rm obs}} |A_i|^2}{\sum_{i=1}^{N_{\rm MC}^{\rm gen}} |A_i|^2}, \tag{2}$$

where $\rm N_{MC}^{gen}$ and $\rm N_{MC}^{obs}$ are the numbers of generated MC events and those passing the event selection, respectively, and A_i is the total amplitude of the ith event.

The Born cross sections are calculated with

$$\sigma_B = \frac{N^{\rm sig}}{\mathcal{L} \times \mathcal{B} \times \epsilon \times (1+\delta^{\rm ISR}) \times \frac{1}{|1-\Pi|^2}}, \tag{3}$$

where $N^{\rm sig}$ is the signal yield with the subtraction of the background contribution, $\mathcal{L}$ is the integrated luminosity, $\mathcal{B}$ is the BF of the decay $K_S^0 \to \pi^+\pi^-$, ϵ is the detection efficiency obtained by incorporating the PWA results as described above, $(1+\delta^{\rm ISR})$ is the ISR correction factor, and $\frac{1}{|1-\Pi|^2}$ is the vacuum polarization factor, which is taken from Ref. [33]. The ISR correction factor is obtained with

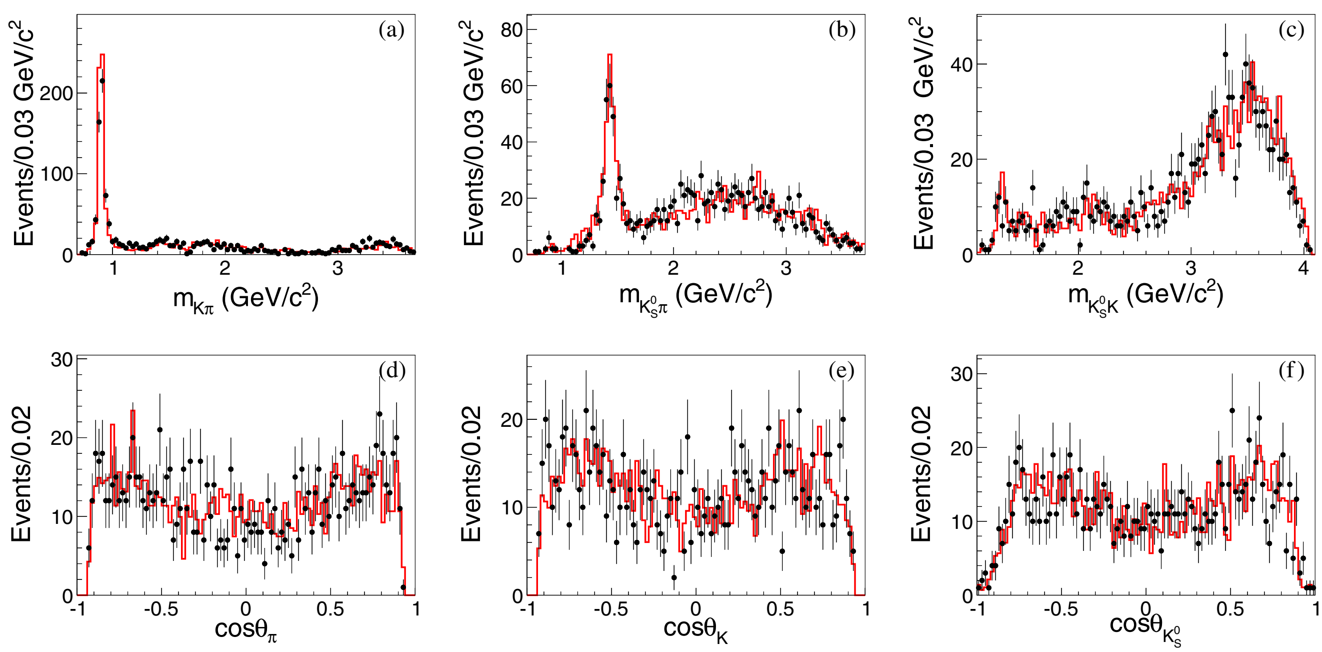

FIG. 3. Comparisons between data and MC simulation at $\sqrt{s} = 4.226$ GeV. The plots (a)-(c) are the invariant mass of $K\pi$, $K_S^0\pi$ and K_S^0K, and the plots (d)-(f) are the polar angle distributions of π, K and K_S^0, respectively. Dots with error bars are data, and the red histograms are the MC projections from the amplitude analysis results.

$$1 + \delta^{\mathrm{ISR}} = \frac{\sigma_{\mathrm{obs}}(s)}{\sigma_B(s)} = \frac{\int \sigma_B(s(1-x))F(x,s)dx}{\sigma_B(s)}, \quad (4)$$

where σ_{obs} is the observed cross section, s is the square of c.m. energy, x is the fraction of the beam energy taken by the radiative photon, and $F(x,s)$ is the radiator function [24]. To get the correct ISR photon energy distribution, the cross section of $e^+e^- \to K_S^0 K^\pm \pi^\mp$ measured by *BABAR* [16] is taken as the input to get the initial ISR correction factor and cross section, the latter is added to recalculate the ISR correction factor. We repeat this process till both the ISR correction factors and cross section converge. The measured Born cross sections for the individual c.m. energy points are summarized in Table I, as well as other quantities used to calculate the Born cross section. A comparison of the Born cross sections between our measurement and *BABAR*'s results in the c.m. energy region $\sqrt{s} =$ 3.800–4.660 GeV is shown in Fig. 4. The measured cross sections agree with but are of much higher precision than those obtained by *BABAR* [16].

The $e^+e^- \to K_S^0 K^+ \pi^-$ Born cross sections of this work are fitted with a $1/s^n$ function. *BABAR*'s [16] results have large uncertainties above 3.8 GeV, so they are not included. In addition, the data point at around 3.8 GeV is not used in the fit, since an attempt to fit the cross section around this energy should consider the contribution from $\psi(3770)$. There is only one data point close to the $\psi(3770)$ peak, which is insufficient to constrain the parameters associated with $\psi(3770)$. The correlations among different data points are considered in the fit, with the chi-square function constructed as Eq. (5), which is minimized by MINUIT [31],

$$\chi^2 = \sum_i \frac{(\sigma_{B_i} - h \cdot \sigma_{B_i}^{\mathrm{fit}})^2}{\delta_i^2} + \frac{(h-1)^2}{\delta_c^2}. \quad (5)$$

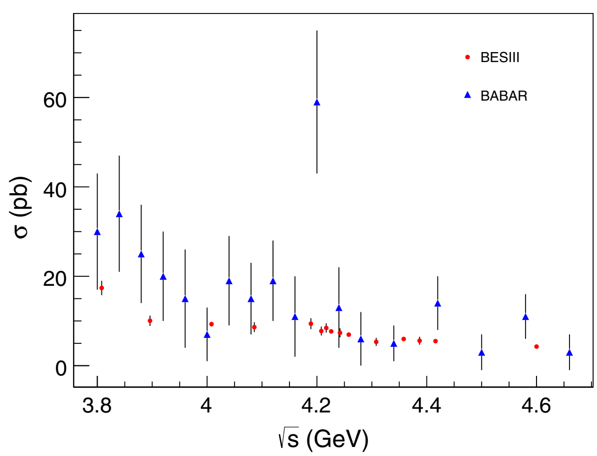

FIG. 4. The $e^+e^- \to K_S^0 K^+ \pi^-$ Born cross sections as a function of $\sqrt{s}$ (red dots) together with the previous results from the *BABAR* experiment [16] (blue triangles). Both statistical and systematic uncertainties are included.

Here, σ_{B_i} and $\sigma_{B_i}^{\mathrm{fit}}$ are the measured and fitted Born cross sections of the ith energy point, respectively; δ_i is the independent part of the total uncertainty, which includes the statistical uncertainty and the uncorrelated part of the systematic uncertainty (the details are in Sec. IV); δ_c is the correlated part of the systematic uncertainty, which will be described in detail in the next section; and h is a free parameter introduced to take into account the correlations. Figure 5(a) shows the fit result with a goodness-of-the-fit of $\chi^2/\mathrm{NDF} = 11.2/12$, where the solid curve shows the continuum process. A better fit is obtained by using the coherent sum of the continuum and the $\psi(4160)$ or $Y(4220)$ amplitude (the two closest states around the excess of the cross section). The fit function used is

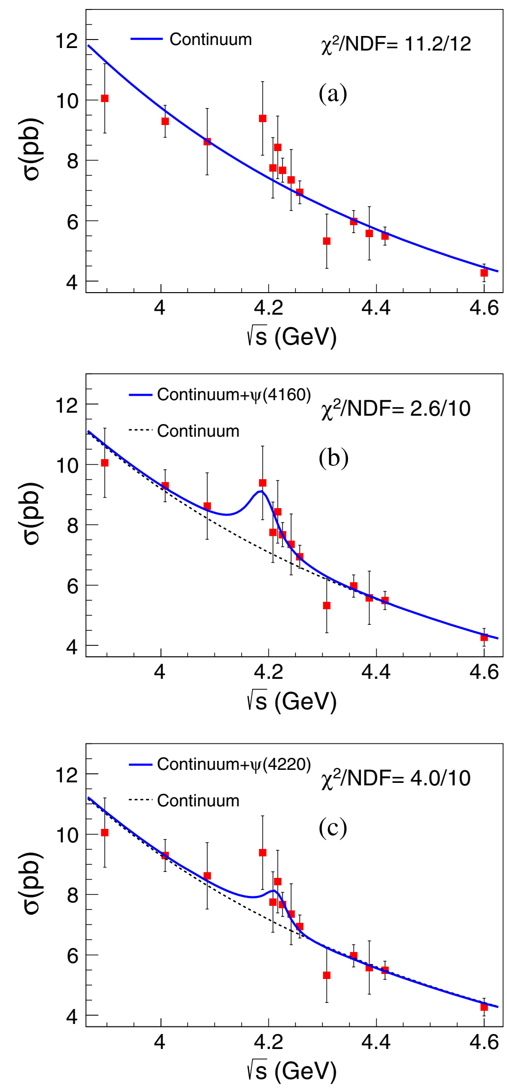

FIG. 5. Fit to the $\sigma_B(e^+e^- \to K_S^0 K^+ \pi^-)$ Born cross section. The data (red squares) include both statistical and systematic uncertainties, the solid curves are the projections from the best fit, and the dashed curves show the fitted continuum components. The top plot is the result with continuum process only, the middle one is with continuum and $\psi(4160)$, and the bottom one is with continuum and $Y(4220)$.

TABLE II. Results of the fits to the Born cross section σ_B. Shown in the table are the product of the e^+e^- partial width and the BF to the $K_S^0K^+\pi^-$ final state $\Gamma_{e^+e^-} \times B_{K_S^0K^+\pi^-}$, the relative phase between the different amplitudes ϕ, and the corresponding significance of $\psi(4160)$ and $Y(4220)$. The uncertainties of the parameters are from the fits.

	$\psi(4160)$		$Y(4220)$	
	Solution I	Solution II	Solution I	Solution II
$\Gamma_{ee} \times B_{K_S^0K^+\pi^-}$ (eV)	2.71 ± 0.13	0.0095 ± 0.0088	2.04 ± 0.19	0.0027 ± 0.0023
ϕ (rad)	-1.60 ± 0.03	1.67 ± 0.44	-1.60 ± 0.02	2.00 ± 0.53
Significance	2.5σ		2.2σ	

$$\sigma = \left| \sqrt{\frac{f_{\mathrm{con}}}{s^n}} + e^{i\phi} \frac{\sqrt{12\pi\Gamma_{e^+e^-}B_{K_S^0K\pi}\Gamma}}{s - M^2 + iM\Gamma} \right|^2, \tag{6}$$

where f_{con} and n are the fit parameters for the continuum process, ϕ is the relative phase between the continuum and resonant amplitudes, Γ and $\Gamma_{e^+e^-}$ are the width and partial width to e^+e^-, respectively, $B_{K_S^0K\pi}$ is the BF of the resonance decays into $K_S^0K^+\pi^-$, and M is the mass of the resonance. The masses and total widths of $\psi(4160)$ and $Y(4220)$ are fixed to Refs. [25,34]. Two solutions with the same minimum value of χ^2 are found with different interference between the two amplitudes. The fit results are shown in Figs. 5(b) and 5(c) (the line shapes of the two solutions are identical) and summarized in Table II. The corresponding significance for $\psi(4160)$ is 2.5σ and for $Y(4220)$ 2.2σ.

IV. SYSTEMATIC UNCERTAINTIES

Various sources of systematic uncertainties are investigated for the cross section measurements of $e^+e^- \to K_S^0K^+\pi^-$, and all of them are summarized in Table III.

The systematic uncertainties associated with tracking and PID have been studied using control samples of $J/\psi \to \pi^+\pi^-p\bar{p}$ and $J/\psi \to K_S^0K^\pm\pi^\mp$ with $K_S^0 \to \pi^+\pi^-$ [35], and the kaon and pion tracking and PID efficiencies for data agree with those of MC simulation within 1%, so the total tracking and PID uncertainties are both determined to be 2% (1.0% per track).

TABLE III. Systematic uncertainties of the measurements of $\sigma(e^+e^- \to K_S^0K^+\pi^-)$.

Source	Relative uncertainty (%)
Tracking	2.0
PID	2.0
K_S^0 reconstruction	1.2
Kinematic fit	0.5
Signal model	2.0
Signal yield	1.8
ISR factor	1.0
Integrated luminosity	1.0
BF	0.1
Total	4.4

The uncertainty associated with K_S^0 reconstruction is studied with the processes $J/\psi \to K^{*\pm}K^\mp$ and $J/\psi \to \phi K_S^0K^\pm\pi^\mp$ [36]. The difference of the reconstruction efficiency between data and MC simulation is found to be 1.2%, which is taken as the systematic uncertainty.

The systematic uncertainty due to the kinematic fit is estimated by correcting the track helix parameters of charged tracks and the corresponding covariance matrix for the signal MC sample to improve the agreement between data and MC simulation. The detailed method can be found in Ref. [37]. The resulting change of the detection efficiency with respect to the one obtained without the corrections is taken as the systematic uncertainty.

In the measurement of the cross section for $e^+e^- \to K_S^0K^+\pi^-$, the detection efficiency is estimated with the weighted PHSP MC samples, where the weights are obtained according to the PWA results. To estimate the corresponding systematic uncertainty associated with the signal MC model, we repeat the PWA by (1) changing the resonance parameters of the intermediate states by one standard deviation [25] and by (2) excluding the intermediate state with the least significance in the fit. The alternative PWA results are used to recalculate the detection efficiency, and the resulting differences are taken as the systematic uncertainties. Assuming the two contributions are uncorrelated, the overall uncertainty associated with the signal MC model is the sum of the above individual values in quadrature. To minimize the effect of the limited statistics of data, the uncertainty for the data sample at $\sqrt{s} = 4.226$ GeV, which has the largest integrated luminosity of all the samples, is used, and the value, 2.0%, is assigned to all c.m. energy points.

For the systematic uncertainties associated with the signal yield determinations, we repeat the analysis by changing the mass interval of $M_{\pi^+\pi^-}$ from 0.03 to 0.04 GeV$/c^2$, and by changing the K_S^0 sideband regions to $m_{\pi^+\pi^-} \in (0.43, 0.45) \cup (0.55, 0.57)$ GeV$/c^2$. The largest change of the signal yields with respect to the nominal value among all c.m. energy points, 1.8%, is conservatively taken as the systematic uncertainty.

The uncertainty associated with the vacuum polarization factor [33] is negligible compared with the other uncertainties. For the ISR correction factors, the iteration procedure is carried out until the measured Born cross section converges. The convergence criterion, 1.0%, is taken as the systematic uncertainty.

The integrated luminosities at each c.m. energy point are measured using large angle Bhabha scattering events with an uncertainty of 1.0% [18]. The uncertainty on the BF of the decay $K_S^0 \to \pi^+\pi^-$ is from the PDG [25].

Assuming all sources of systematic uncertainties are uncorrelated, the total systematic uncertainty is obtained by adding the individual values in quadrature and are summarized in Table III.

V. SUMMARY

The $e^+e^- \to K_S^0 K^\pm \pi^\mp$ Born cross sections have been measured by BESIII at the c.m. energy region from 3.8 to 4.6 GeV, and the results are shown in Fig. 4 and summarized in Table I. The cross sections agree with *BABAR*'s results [16], but with significantly improved precision. The line shape of the Born cross sections is consistent with only the continuum process, however a better fit is obtained by adding an additional resonance. The fit to the Born cross sections from this work, with $\psi(4160)$ [$Y(4220)$] added, is performed. Only evidence for the $\psi(4160)$ [$Y(4220)$] is observed with the corresponding significance 2.5σ (2.2σ). Further study of this channel with more energy points and larger statistics will be essential for a deeper understanding of the line shape and contributions from charmonium and charmoniumlike states.

ACKNOWLEDGMENTS

The BESIII collaboration thanks the staff of BEPCII and the IHEP computing center for their strong support. This work is supported in part by National Key Basic Research Program of China under Contract No. 2015CB856700; National Natural Science Foundation of China (NSFC) under Contracts No. 11235011, No. 11335008, No. 11425524, No. 11625523, No. 11635010; the Chinese Academy of Sciences (CAS) Large-Scale Scientific Facility Program; the CAS Center for Excellence in Particle Physics (CCEPP); Joint Large-Scale Scientific Facility Funds of the NSFC and CAS under Contracts No. U1332201, No. U1532257, No. U1532258; CAS under Contracts No. KJCX2-YW-N29, No. KJCX2-YW-N45; CAS Key Research Program of Frontier Sciences under Contracts No. QYZDJ-SSW-SLH003, No. QYZDJ-SSW-SLH040; 100 Talents Program of CAS; National 1000 Talents Program of China; INPAC and Shanghai Key Laboratory for Particle Physics and Cosmology; German Research Foundation DFG under Contracts Nos. Collaborative Research Center CRC 1044, FOR 2359; Istituto Nazionale di Fisica Nucleare, Italy; Koninklijke Nederlandse Akademie van Wetenschappen (KNAW) under Contract No. 530-4CDP03; Ministry of Development of Turkey under Contract No. DPT2006K-120470; National Science and Technology fund; The Swedish Research Council; U.S. Department of Energy under Contracts No. DE-FG02-05ER41374, No. DE-SC-0010118, No. DE-SC-0010504, No. DE-SC-0012069; University of Groningen (RuG) and the Helmholtzzentrum fuer Schwerionenforschung GmbH (GSI), Darmstadt; WCU Program of National Research Foundation of Korea under Contract No. R32-2008-000-10155-0.

[1] B. Aubert *et al.* (*BABAR* Collaboration), Phys. Rev. Lett. **95**, 142001 (2005).
[2] Q. He *et al.* (CLEO Collaboration), Phys. Rev. D **74**, 091104(R) (2006).
[3] C. Z. Yuan *et al.* (Belle Collaboration), Phys. Rev. Lett. **99**, 182004 (2007).
[4] M. Ablikim *et al.* (BESIII Collaboration), Phys. Rev. Lett. **118**, 092002 (2017).
[5] M. Ablikim *et al.* (BESIII Collaboration), Phys. Rev. Lett. **118**, 092001 (2017).
[6] E. Eichten, K. Gottfried, T. Kinoshita, K. D. Lane, and T. M. Yan, Phys. Rev. D **17**, 3090 (1978).
[7] E. Eichten, K. Gottfried, T. Kinoshita, K. D. Lane, and T. M. Yan, Phys. Rev. D **21**, 203 (1980).
[8] T. Barnes, S. Godfrey, and E. S. Swanson, Phys. Rev. D **72**, 054026 (2005).
[9] X. H. Mo, G. Li, C. Z. Yuan, K. L. He, H. M. Hu, J. H. Hu, P. Wang, and Z. Y. Wang, Phys. Lett. B **640**, 182 (2006).
[10] F. K. Guo, C. Hanhart, and U. G. Meißner, Q. Wang, Q. Zhao, and B. S. Zou, Rev. Mod. Phys. **90**, 015004 (2018).
[11] A. Esposito, A. Pilloni, and A. D. Polosa, Phys. Rep. **668**, 1 (2017).
[12] R. F. Lebed, R. E. Mitchell, and E. S. Swanson, Prog. Part. Nucl. Phys. **93**, 143 (2017).
[13] H. X. Chen, W. Chen, X. Liu, and S. L. Zhu, Phys. Rep. **639**, 1 (2016).
[14] D. Y. Chen, X. Liu, X. Q. Li, and H. W. Ke, Phys. Rev. D **93**, 014011 (2016).
[15] T. E. Coan *et al.* (CLEO Collaboration), Phys. Rev. Lett. **96**, 162003 (2006).
[16] B. Aubert *et al.* (*BABAR* Collaboration) Phys. Rev. D **77**, 092002 (2008).
[17] M. Ablikim *et al.* (BESIII Collaboration), Chin. Phys. C **40**, 063001 (2016).
[18] M. Ablikim *et al.* (BESIII Collaboration), Chin. Phys. C **39**, 093001 (2015).

[19] M. Ablikim *et al.* (BESIII Collaboration), Nucl. Instrum. Methods Phys. Res., Sect. A **614**, 345 (2010).
[20] C. Zhang, Sci. Chin. Phys. Mech. Astron. **53**, 2084 (2010).
[21] S. Agostinelli *et al.*, Nucl. Instrum. Methods Phys. Res., Sect. A **506**, 250 (2003).
[22] R. G. Ping, Chin. Phys. C **32**, 599 (2008).
[23] D. J. Lange, Nucl. Instrum. Methods Phys. Res., Sect. A **462**, 152 (2001).
[24] E. A. Kuraev and V. S. Fadin, Sov. J. Nucl. Phys. **41**, 466 (1985) [Yad. Fiz. **41**, 733 (1985)].
[25] C. Patrignani *et al.* (Particle Data Group), Chin. Phys. C **40**, 100001 (2016).
[26] J. C. Chen, G. S. Huang, X. R. Qi, D. H. Zhang, and Y. S. Zhu, Phys. Rev. D **62**, 034003 (2000).
[27] M. Xu *et al.*, Chin. Phys. C **33**, 428 (2009).
[28] S. U. Chung, Phys. Rev. D **57**, 431 (1998).
[29] S. U. Chung, Phys. Rev. D **48**, 1225 (1993).
[30] B. S. Zou and D. V. Bugg, Eur. Phys. J. A **16**, 537 (2003).
[31] F. James, Comput. Phys. Commun. **10**, 343 (1975).
[32] M. Ablikim *et al.* (BESIII Collaboration), Phys. Rev. D **86**, 072011 (2012).
[33] S. Actis *et al.*, Eur. Phys. J. C **66**, 585 (2010).
[34] X. Y. Gao, C. P. Shen, and C. Z. Yuan, Phys. Rev. D **95**, 092007 (2017).
[35] M. Ablikim *et al.* (BESIII Collaboration), Phys. Rev. D **83**, 112005 (2011).
[36] M. Ablikim *et al.* (BESIII Collaboration), Phys. Rev. D **92**, 112008 (2015).
[37] M. Ablikim *et al.* (BESIII Collaboration), Phys. Rev. D **87**, 012002 (2013).